Acta Cryst B
STRUCTURAL SCIENCE
CRYSTAL ENGINEERING
MATERIALS

ISSN 2052-5206

The crystal structure of cesbronite, $Cu_3TeO_4(OH)_4$: a novel sheet tellurate topology

O. P. Missen,[a,b]* S. J. Mills,[a] M. D. Welch,[c] J. Spratt,[d] M. S. Rumsey,[c] W. D. Birch[a] and J. Brugger[e]

[a]Geosciences, Museums Victoria, GPO Box 666, Melbourne, Victoria 3001, Australia, [b]School of Chemistry, University of Melbourne, Victoria, 3010, Australia, [c]Department of Earth Sciences, Natural History Museum, Cromwell Road, London, SW7 5BD, UK, [d]Department of Core Research Laboratories, Natural History Museum, Cromwell Road, London, SW7 5BD, UK, and [e]School of Earth, Atmosphere and the Environment, Monash University, Clayton, Victoria 3800, Australia. *Correspondence e-mail: omissen@museum.vic.gov.au

Received 2 October 2017
Accepted 15 November 2017

Edited by S. Parsons, University of Edinburgh, Scotland

Keywords: cesbronite; crystal structure; tellurate; xocomecatlite; oxysalt; electron-microprobe analysis; powder diffraction; single-crystal X-ray diffraction; Raman spectroscopy.

Supporting information: this article has supporting information at journals.iucr.org/b

The crystal structure of cesbronite has been determined using single-crystal X-ray diffraction and supported by electron-microprobe analysis, powder diffraction and Raman spectroscopy. Cesbronite is orthorhombic, space group *Cmcm*, with a = 2.93172 (16), b = 11.8414 (6), c = 8.6047 (4) Å and V = 298.72 (3) Å^3. The chemical formula of cesbronite has been revised to $Cu^{II}_3Te^{VI}O_4(OH)_4$ from $Cu^{II}_5(Te^{IV}O_3)_2(OH)_6{\cdot}2H_2O$. This change has been accepted by the Commission on New Minerals, Nomenclature and Classification of the International Mineralogical Association, Proposal 17-C. The previously reported oxidation state of tellurium has been shown to be incorrect; the crystal structure, bond valence studies and charge balance clearly show tellurium to be hexavalent. The crystal structure of cesbronite is formed from corrugated sheets of edge-sharing CuO_6 and $(Cu_{0.5}Te_{0.5})O_6$ octahedra. The structure determined here is an average structure that has underlying ordering of Cu and Te at one of the two metal sites, designated as *M*, which has an occupancy $Cu_{0.5}Te_{0.5}$. This averaging probably arises from an absence of correlation between adjacent polyhedral sheets, as there are two different hydrogen-bonding configurations linking sheets that are related by a $\frac{1}{2}a$ offset. Randomised stacking of these two configurations results in the superposition of Cu and Te and leads to the $Cu_{0.5}Te_{0.5}$ occupancy of the *M* site in the average structure. Bond-valence analysis is used to choose the most probable Cu/Te ordering scheme and also to identify protonation sites (OH). The chosen ordering scheme and its associated OH sites are shown to be consistent with the revised chemical formula.

1. Introduction

Tellurium minerals comprise a surprisingly large portion of the mineralogical record (*e.g.* Christy, Mills & Kampf, 2016; Christy, Mills, Kampf *et al.*, 2016; Grundler *et al.*, 2008). Tellurium is found as a native element, as tellurides, and as tellurium oxysalts (Christy, Mills & Kampf, 2016; Christy, Mills, Kampf *et al.*, 2016). Over 150 tellurium minerals have been recorded, and abundant sources of new oxysalt minerals such as those at the Otto Mountain mine in California have only been discovered since the year 2000 (*e.g.* Kampf, Housley, Mills *et al.*, 2010; Kampf *et al.*, 2016). Secondary tellurium minerals featuring two tellurium oxidation states, +IV and +VI, typically form from alteration of sulfide zones rich in tellurides under conditions of high E_h and pH (Mills *et al.*, 2014; Grundler *et al.*, 2008). The availability of two stable oxidation states contributes to their observed diversity. Eleven tellurium oxysalt minerals containing copper as the sole other cation are known (Pasero, 2017). These minerals include examples of Te^{IV} and Te^{VI}, anhydrous and hydrated minerals, and different coordination numbers of both copper and tell-

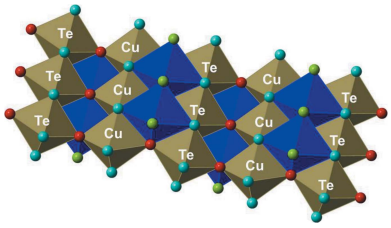

urium, showing the diversity of structures that these elements are able to form together.

Cesbronite is a rare secondary tellurium mineral found in only a few North American localities (Williams, 1974; Roberts *et al.*, 1997). It is one of many tellurium oxysalt minerals first recognised from the Moctezuma, Bambolla, Bambollita and Oriental mines of Sonora, Mexico (Gaines, 1970; Grundler *et al.*, 2008). Cesbronite was described without a crystal structure (Williams, 1974) as no suitable crystals were found for single-crystal study. The formula was reported as $Cu^{II}_5(Te^{IV}O_3)_2(OH)_6{\cdot}2H_2O$, with the tellurium oxidation state determined by a microchemical test.

2. Specimen descriptions

The specimen of cesbronite from which the single crystal was isolated for X-ray diffraction analysis was found amongst several kilograms of material collected from the dumps of the Moctezuma mine, Sonora, Mexico (29°48′ N, 109°40′ W) in 2004 by one of the authors (JB) and is registered in the collections of Museums Victoria, registration number M53919. This cesbronite specimen is arguably the highest quality cesbronite in the world, and was found to contain around 50 clusters of bright emerald-green cesbronite crystals (see Fig. 1), typically nestled in cavities amongst quartz. Cesbronite occurs as complex stepped subparallel intergrowths up to 0.3 mm in diameter in which an individual 'tooth' is itself an aggregate of stacked small, thin, platy crystals less than 0.05 mm in thickness. Individual plates can be extracted by careful manipulation due to the well developed {010} cleavage. Clusters readily separate into crystalline aggregates upon removal from parent material. No twinning was observed.

Two other cesbronite specimens from the National History Museum, London collection (the cotype specimen, BM 1976,405; and also BM 1980,432) had been examined. The cotype specimen contained only two major clusters of cesbronite, whereas BM 1980,432 contained around 20. Both of these specimens contained cesbronite clusters which were smaller (<0.2 mm diameter) and of poorer crystallinity than M53919, although they were used for microprobe analysis. The xocomecatlite cotype specimen (BM 1976,404) was also found to contain several cesbronite aggregates. A cesbronite crystal from BM 1976,405 was mounted and analysed at the MX2 beamline of the Australian Synchrotron. Due to the poor quality, the crystal structure could not be determined; however, the orthorhombic unit cell of a = 2.93, b = 11.84 and c = 8.60 Å was determined and thus used for verification purposes.

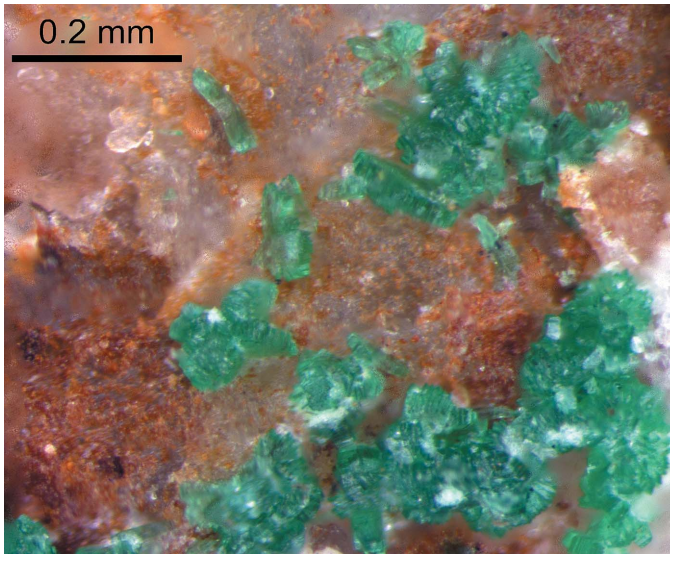

Figure 1
Pale emerald-green crystalline aggregates of cesbronite on M53919.

Table 1
The average composition of cesbronite determined by electron probe micro-analysis and structure determination.

Specimen 1: BM 1976,405, 12 analyses; specimen 2: BM 1980,432, 22 analyses.

	Specimen 1				Specimen 2			
Oxide	Avg	Min	Max	Std dev.	Avg	Min	Max	Std dev.
CaO	0.12	0.07	0.17	0.03	–	–	–	–
CuO	50.6	49.8	51.8	0.53	50.0	49.3	50.9	0.44
ZnO	1.0	0.5	1.5	0.28	1.2	0.8	1.5	0.21
TeO_3	37.7	36.7	38.6	0.50	39.3	38.8	39.9	0.28
PbO	0.8	0.3	1.0	0.20	-	–	–	-
H_2O†	7.80	7.74	7.89	0.05	7.90	7.84	7.99	0.04
Total	98.07				98.45			

† Calculated based on the crystal structure (using eight total anions per formula unit as a reference).

3. Chemistry

Quantitative chemical analyses of cesbronite were performed on a Cameca SX100 Electron Microprobe (WDS mode, 12 kV, 10 nA, 5 μm beam diameter and PAP matrix correction) at the Imaging and Analysis Centre, Core Research Laboratories, Natural History Museum, London. The standards used were: wollastonite (Ca), Cu_2O (Cu), sphalerite (Zn), TeO_2 (Te) and vanadinite (Pb). Results are recorded to only one decimal place for Cu, Zn, Te and Pb as the low values of voltage and current used to reduce dehydration during analysis input less energy into the sample and, consequently, give lower counting statistics for these elements. Analytical results are given in Table 1. Two specimens of cesbronite were analysed (BM 1976,405 and BM 1980,432); these were almost identical except that BM 1976,405 contained minor Ca and Pb. No other elements were detected using EDS or EMPA. There was insufficient cesbronite for CHN analyses, therefore H_2O was calculated based on four total cations (3 Cu + 1 Te) and eight total anions (4 O + 4 OH) per formula unit (p.f.u), determined by the crystal structure analysis (see below). A small amount of sample dehydration was observed but the totals, exceeding 98% including calculated H_2O, were not significantly affected.

The analyses show that cesbronite contains only two essential metallic cations, namely copper and tellurium. The empirical formula (based on 8 O and 4 H atoms p.f.u.) for BM 1976,405 is $Cu_{2.94}Zn_{0.06}Pb_{0.02}Ca_{0.01}Te_{0.99}H_{4.00}O_{8.00}$ and for BM

1980,432 is $Cu_{2.87}Zn_{0.07}Te_{1.02}H_{4.00}O_{8.00}$. The ideal formula, based on the OH content inferred from crystal structure determination, is $Cu^{II}{}_3Te^{VI}H_4O_8$, *i.e.* $Cu^{II}{}_3Te^{VI}O_4(OH)_4$. This requires CuO 53.00, TeO_3 39.00 and H_2O 8.00, total 100 wt%.

In comparison with the original data presented by Williams (1974), CuO is within error of our analysed value. Williams calculated Te incorrectly as TeO_2, obtaining 38.9 wt% (with a standard deviation of 0.4 wt%); as TeO_3 the value should have been 42.8 (0.4) wt%. This value is significantly higher than the TeO_3 values reported in this study, 37.7 (0.5) and 39.3 (0.3) wt% for BM 1976,405 and BM 1980,432, respectively. None of the Zn, Ca and Pb found in this study were reported by Williams (1974). Lower totals led Williams (1974) to assign an overly high degree of hydration. Due to the inaccuracies associated with scraping enough pure material from type specimens for bulk chemical analyses, several tellurium (*e.g.* girdite; Kampf *et al.*, 2017) and other secondary minerals (*e.g.* mendozavilite and paramendozavilite; Kampf *et al.*, 2012) have had to be closely re-examined, and in the case of girdite, discredited.

4. Raman spectroscopy

The Raman spectrum (Fig. 2) of cesbronite was recorded from a crystal cluster located on BM 1976,405 without removing any aggregates from the specimen. The spectrum was obtained using a Renishaw Invia spectrometer with an argon ion laser excitation operating at 514 nm. The spot was about 1 μm in diameter, with a 20 cm s^{-1} scan rate and about 1 mW at the sample when using 10% laser power.

The Raman data showed a main peak at 687 cm^{-1} with a shoulder at 633 cm^{-1}, which can be assigned to Te^{VI}—O stretching vibrations. These bands are similar to those observed in thorneite (~700 cm^{-1}; Kampf, Housley & Marty, 2010), bairdite (721 cm^{-1}; Kampf *et al.*, 2013*a*), eckhardite (729 cm^{-1}; Kampf *et al.*, 2013*b*), and andychristyite (706 cm^{-1}; Kampf *et al.*, 2016). Frost & Keeffe (2009) undertook a Raman spectroscopic study of the mineral xocomecatlite [reported as Te^{VI}]; however, until more is known about the chemistry of xocomecatlite, this study cannot be reliably used for comparison with the Raman spectrum of cesbronite. No evidence for O—H stretches was observed, despite the presence of OH groups confirmed in the crystal structure below. The H—O—H bend was absent around the 1600 cm^{-1} region, consistent with the absence of H_2O in cesbronite. A complete assignment of probable Raman peaks is given in Table 2.

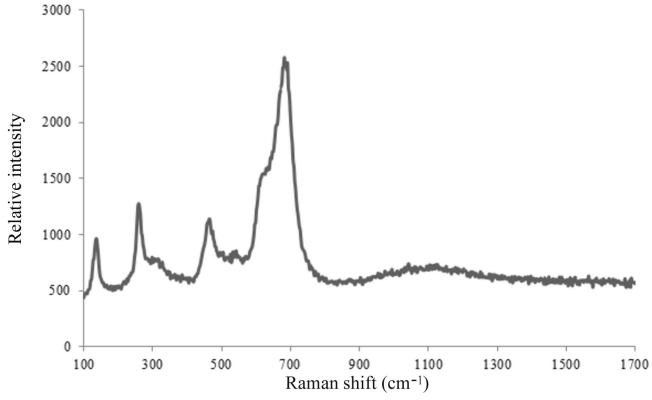

Figure 2
Raman spectrum of cesbronite.

Table 2
Raman bands assignment for cesbronite (BM 1976,405 specimen).

Wavenumbers (cm^{-1})	Probable assignment
687 (most intense)	$\nu1$ $(TeO_6)^{6-}$ symmetric stretch
633 (shoulder of most intense peak)	$\nu3$ $(TeO_6)^{6-}$ antisymmetric stretch
542 (minor)	M—O lattice modes
464	M—O lattice modes
316 (minor)	$\nu2$ $(TeO_6)^{6-}$ symmetric bend
260	$\nu4$ $(TeO_6)^{6-}$ antisymmetric bend
137	M—O lattice modes

5. Crystallography

5.1. Powder diffraction

An aggregate of cesbronite obtained from the BM 1976,404 specimen was mounted on a Rigaku *R*-Axis curved imaging plate diffractometer (Rigaku Oxford Diffraction) and a dataset collected using Cu $K\alpha$ radiation. A Gandolfi-type randomised crystal movement was achieved by rotations on the φ and ω axes. Observed d_{hkl} and reflection intensities collected to 2θ = 90° were derived by profile-fitting using *Highscore Plus* software (Degen *et al.*, 2014). The unit-cell parameters refined using *Chekcell* (Laugier & Bochu, 2004) from the powder data are a = 2.937 (1), b = 11.900 (3), c = 8.621 (3) Å and V = 301.3 (3) $Å^3$. These values are in good agreement with the synchrotron single crystal cell obtained for the cotype (see *Specimen descriptions*, above) and with the pattern calculated using the *PowderCell* program (Kraus & Nolze, 1996) from the single-crystal structure (shown in Table 3). The powder data as indexed by Williams (1974) gave the orthorhombic cell a = 8.624, b = 11.878, c = 5.872 Å and V = 601.5 $Å^3$. The relationship between this cell and ours is $\frac{1}{2}c$, b, a. These powder lines are readily indexed using our new cell, and there is no need for doubling of the c axis (a in our setting).

5.2. Single-crystal X-ray diffraction

A composite crystal from M53919 comprising two components was attached to a non-diffracting amorphous-carbon fibre (10 μm diameter) that was glued to a glass support rod. Diffraction data were collected using an Xcalibur four-circle X-ray diffractometer equipped with an EoS area detector (both by Rigaku Oxford Diffraction, 2015) at the Natural History Museum, London. Graphite-monochromated Mo $K\alpha$ radiation (45 kV and 40 mA) was used. Details of the data collection are summarised in Table 3.

A full sphere of reflection data was collected to θ = 32.65° with 100% completeness to θ = 30°. Inspection of reconstructed diffraction patterns showed clearly that there were two components to the crystal. The misorientation of the two components is a small rotational offset about the y axis, rather

Table 3
Summary of information relating to data collection and structure refinement of cesbronite.

Crystal data	
Ideal chemical formula	$Cu_3TeO_4(OH)_4$
Space group	*Cmcm*
a (Å)	2.93172 (16)
b (Å)	11.8414 (6)
c (Å)	8.6047 (4)
V (Å^3)	298.72 (3)
Z	2
D_x (Mg m^{-3})	4.961
μ (mm^{-1})	15.372
Crystal size (mm)	0.045 × 0.025 × 0.015
Crystal description	Emerald-green, transparent, triangular plate
Data collection	
Diffractometer	Xcalibur E (1K Eos detector)
Radiation, wavelength (Å)	Mo *Kα*, 0.71073
Temperature (K)	293 (1)
Scan type, frame-width (°), frame-time (s)	*ω*, 1, 180
Absorption correction	Multi-scan (*ABSPACK*)
T_{min}, T_{max}	0.809, 1
No. of reflections used for cell, $I > 7\sigma(I)$	857
No. of reflections components 1, 2, overlapped†	2463, 2469, 345
R_σ	0.0396
No. of independent reflections (HKLF5 file)‡	763
No. of independent reflections with $I > 2\sigma(I)$	649
θ_{min}, θ_{max} (°)	3.44, 32.65
Index range	$h \pm 4$, $k \pm 17$, $l \pm 12$
Data completeness to θ = 30° (%)	100
Crystal structure refinement	
No. of independent reflections, restraints, parameters	326, 0, 25
R_{int}	0.062
R_1 [$I > 2\sigma(I)$], R_1 (all)	0.0321, 0.0436
wR_2 [$I > 2\sigma(I)$], wR_2 (all)	0.0663, 0.0682
GoF (F^2)	1.036
SHELX reflection weighting coefficients *a*, *b*	0.0378, 0
$(\Delta/\sigma)_{max}$	<0.001
$\Delta\rho_{max}$, $\Delta\rho_{min}$ (e Å^{-3})	1.45, −2.09

† 345 reflections with <80% overlap were used. ‡ See text for discussion.

than twinning. This rotational offset is consistent with the pervasive {010} cleavage of cesbronite, *i.e.* the two components of the crystal are divided along the most prominent cleavage plane. Reflection intensities were integrated, corrected for Lorentz and polarisation effects and converted to structure factors using the program *CrysAlis PRO* (Rigaku Oxford Diffraction, 2015). A single-component reflection file (HKLF4) and a dual-component reflection file (HKLF5) were obtained (Sheldrick, 2008). The initial twin scale factor (BASF) output by *CrysAlis PRO* was 0.4974, which indicates that the two components are present in nearly equal amounts.

Systematic absences are most consistent with the space group *Cmcm*. Reflection merging for each of the two components in Laue group *mmm* gave R_{int} values of 0.061 and 0.065 for separated reflections, and 0.045 for the 345 overlapping reflections with <80% overlap. The total R_{int} is 0.062. All values are acceptable for such small crystals. Consequently, the full dataset to θ = 32.65° was used without truncation.

Solution and refinement in *Cmcm* produced a very well defined crystal with a chemically plausible structure. The single-component reflection file was used for structure solution followed by use of the dual-component reflection file for structure refinement. Structure solution was carried out by direct methods using *SHELXS* (Sheldrick, 2008) and structure refinement by full-matrix least-squares was implemented by *SHELXL* (Sheldrick, 2015). Neutral atomic scattering factors were used for all atoms.

The presence of two components in the crystal means that multiple values for some F_0 are present in the dataset. Consequently, the number of reflections listed in Table 3 refers to those dual-components in the input file. The final value of merging at convergence (R_{merge}) was 0.037 for 326 independent reflections.

Structure solution in space group *Cmcm* located one Cu, one Te and three O atoms in the asymmetric unit. It was observed that the U_{iso} value of the Te site was much larger than that of the Cu site, indicative of the presence of a lower electron count than expected for full occupancy by Te. To check electron counts, the occupancy levels of the Cu and Te sites were refined, initially using just Cu and Te scattering factors, respectively. At this stage the occupancy of the Cu site refined to 95 (2)% and the Te site to 74 (2)%. The latter corresponds to 38 electrons, a value close to 50%Cu + 50%Te occupancy (41 electrons). We refer to this mixed site as the *M* site. As the refined occupancy of the Cu site was very close to being full (28 electrons), its occupancy was fixed at unity for subsequent least-squares anisotropic refinement. Refinement of the joint occupancy of the *M* site led to a final occupancy 0.509 (9) Cu + 0.491 (9) Te, clearly demonstrating $Cu_{0.5}Te_{0.5}$ composition. All atom positions, anisotropic displacement parameters (U_{ij}) and the occupancy of the *M* site were refined with reflection weighting and converged to final R_1 and wR_2 values of 0.0321 and 0.0663, respectively. Extinction was not refined (it was not indicated by residual F_{obs}/F_{calc} values). Atom coordinates and displacement parameters are given in Table 4. Bond distances are shown in Table 5 and a bond valence analysis is shown in Table 6, using the bond valence parameters of Mills & Christy (2013) for Te, and Gagné & Hawthorne (2015) for Cu.

5.3. Crystal stucture description

The crystal structure of cesbronite (Figs. 3–7) is novel and the mineral has no synthetic analogue. *M*-site atoms form four near-coplanar *M*—O3 bonds of 1.948 (3) Å and two longer *M*—O1 bonds of 2.1992 (17) Å. These long bonds are oriented *trans* to the planar MO_4 square, such that the MO_6 site displays prolate octahedral configuration. Each MO_6 octahedral site is connected to its neighbouring MO_6 site along **c** *via* corner sharing of the apical O1 atoms (Fig. 3). The O1 site has a strongly anisotropic displacement ellipsoid (Fig. 4), the centre of which is 2.1992 (17) Å from *M*, due to the presence of Jahn–Teller distorted Cu^{II} in half of these sites. The average length of a Te^{VI}—O apical bond reported by Mills & Christy

Table 4
Atom coordinates, site occupancies and atomic displacement parameters (Å^2) for cesbronite.

Atom	*x*/*a*	*y*/*b*	*z*/*c*	Occ.	U_{eq}	U_{11}	U_{22}	U_{33}	U_{23}	U_{13}	U_{12}
Cu1	0	0.35007 (10)	$\frac{3}{4}$	1	0.0076 (3)	0.0051 (5)	0.0085 (6)	0.0092 (5)	0	0	0
Cu2	$-\frac{1}{2}$	$\frac{1}{2}$	$\frac{1}{2}$	0.51 (1)	0.0061 (2)	0.0039 (3)	0.0078 (4)	0.0066 (3)	0.0005 (3)	0	0
Te2	$-\frac{1}{2}$	$\frac{1}{2}$	$\frac{1}{2}$	0.49 (1)	0.0061 (2)	0.0039 (3)	0.0078 (4)	0.0066 (3)	0.0005 (3)	0	0
O1	$-\frac{1}{2}$	0.4614 (7)	$\frac{3}{4}$	1	0.038 (2)	0.008 (3)	0.008 (3)	0.097 (8)	0	0	0
O2	$-\frac{1}{2}$	0.2384 (5)	$\frac{3}{4}$	1	0.0086 (12)	0.005 (3)	0.009 (3)	0.011 (3)	0	0	0
O3	−1	0.3928 (4)	0.4789 (4)	1	0.0087 (9)	0.0097 (19)	0.008 (2)	0.008 (2)	0.0002 (16)	0	0

Table 5
Metal—oxygen bond lengths (Å) for cesbronite.

Cu1—O1 (×2)	1.971 (5)	Cu2—O3 (×4)†	1.948 (3)	Cu2—O3 (×4)‡	1.948 (3)
Cu1—O2 (×2)	1.974 (4)	Cu2—O1 (×2)	2.1992 (17)	Cu2—O1′ (×2)	2.49
Cu1—O3 (×2)	2.387 (4)	⟨Cu2—O⟩	2.032	⟨Cu2—O′⟩	2.129
⟨Cu1—O⟩	2.111				
		Te2—O3 (×4)	1.948 (3)	Te2—O3 (×4)	1.948 (3)
		Te2—O1 (×2)	2.1997 (17)	Te2—O1′ (×2)	1.91
		⟨Te2—O⟩	2.032	⟨Te2—O′⟩	1.935

† Note: values without foci (*M* sites, *i.e.* Cu2 and Te2 in the central column) do not incorporate the ellipsoid foci, instead treating O1 as a single site 2.1992 (17) Å from the *M* site. ‡ The right-hand

Table 6
Bond valence sums (in valence units) for cesbronite.

Primes indicate columns in which focal ellipsoid lengths are used.

	Cu1	*M* site	Te2′	Cu2′	Σ (no foci)	Σ (with foci)
O1	0.449 (×2)	0.422 (×2)	1.020 (×2 ↓)	0.104 (×2 ↓)	1.743	2.023
O2	0.446 (×2)				0.891	0.891
O3	0.139 (×2 ↓)	0.717 (×4 ↓, ×2 →)	0.953 (×4 ↓)	0.480 (×4 ↓)	1.572†	1.572
Σ	2.068	3.711	5.853	2.128		

† Note: 1.572 v.u. is the bond valence obtained for ordering scheme (1), $1Te_S + 1Cu_S + 1Cu_L$. Using ordering scheme (2) the values obtained are 1.099 v.u. for the OH site ($2Cu_S + 1Cu_L$ triplet) and 2.046 v.u. for the unprotonated O ($2Te_S + 1Cu_L$ triplet). The average bond valence at this site for both ordering schemes is 1.572 v.u., however, ordering scheme (2) better explains the location of H atoms in cesbronite.

(2013) is 1.923 ± 0.041 Å, and the typical Cu—O apical bond is ∼2.44 Å (Eby & Hawthorne, 1993).

The presence of this anisotropy is consistent with the mixed occupancy of the *M* site, *i.e.* the anisotropy reflects the different lengths of Te—O and Cu—O apical bonds (Fig. 4). Each focus of the ellipsoid is 0.29 Å from the centroid, and the two *M*—O distances to a focus are ∼1.91 and ∼2.49 Å, which we attribute to Te—O and Cu—O bonds, respectively. The absence of significant positional anisotropy for O3 atoms can be explained by the very similar 'equatorial' bond lengths for Cu—O (typically ∼1.97 Å; Eby & Hawthorne, 1993) and Te^{VI}—O (1.923 ± 0.041 Å; Mills & Christy, 2013) in oxysalt compounds.

A second octahedrally coordinated metal site shares an edge with each of two neighbouring MO_6 octahedra. This Cu1 site is in typical Jahn–Teller configuration and is fully occupied by Cu. The four short Cu—O bonds are two pairs having lengths of 1.971 (5) and 1.974 (4) Å and the apical bonds of this site are to O3 at 2.387 (4) Å. Alternating rows of $Cu1O_6$ and MO_6 octahedra extend parallel to [100] and share edges to form an infinite sheet parallel to (010). Below we present a model for the ordering of Cu and Te in cesbronite associated with the *M* site. In this model we also identify that O2 and O3 atoms are OH groups. Although we cannot locate H atoms from the X-ray data for the very small crystal, it is clear from bond valence analysis (see below) that these two O atoms are OH groups and that the polyhedral sheets are connected *via* hydrogen bonding.

5.4. The average structure

Successive polyhedral sheets of cesbronite (Fig. 5) are displaced by $\frac{1}{2}a$ and $\frac{1}{2}c$, as the reflection across the *c*-glide is maintained. One of the two cation sites of cesbronite (the *M* site) is mixed $Cu_{0.5}Te_{0.5}$. There is no evidence for doubling of *a* or *c* lattice parameters that would arise if there was correlation of the occupancy of the *M* site (long-range ordering) between adjacent sheets. As we describe below, the very different oxidation states of Cu and Te in cesbronite imply that there will be strong ordering of these cations within a sheet due to bond-valence constraints.

Later, we describe the two possible inter-sheet hydrogen-bonding configurations that lead to the average structure. We propose that the average structure arises from an absence of correlation between Cu and Te sites between adjacent polyhedral sheets due to the two similar but topologically distinct hydrogen-bonding schemes. We now consider the significance of Cu/Te ordering within sheets for the formula of cesbronite and show that a clear choice can be made between two contrasting ordering schemes that also identifies OH groups. The chosen ordering scheme does not require doubling of *b* or *c* parameters.

5.5. Ordering of Cu and Te at the mixed site

Two very different ordering schemes can be considered: (1) Cu and Te alternate along a row parallel to [100] (Fig. 6*a*); (2) Cu and Te as separate Te and Cu [100] rows (Fig. 6*b*).

5.6. OH in cesbronite

The cesbronite formula has twelve positive charges and there are eight O atoms p.f.u. (16 O atoms in the unit cell, $Z = 2$). Consequently, four positive charges are needed for a

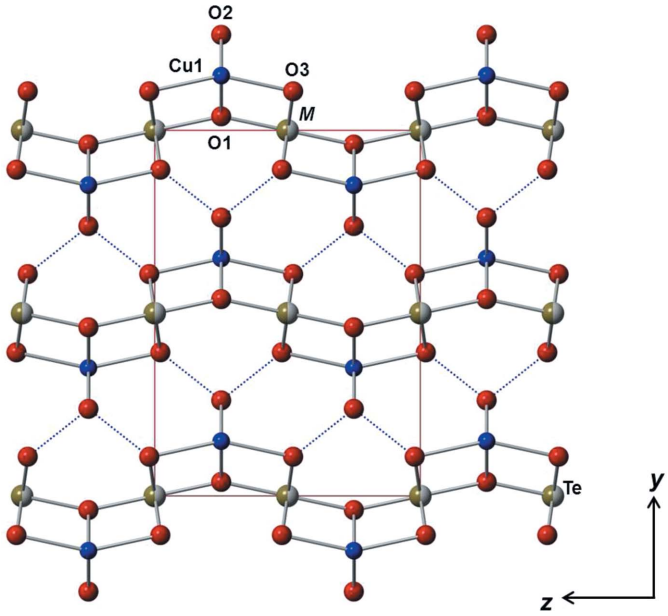

Figure 3
Ball-and-stick model of the cesbronite average structure viewed along **a**. The oxygen atoms are red, the Cu1 site is cyan, and the *M* site (on average 50% Te and 50% Cu) is shown as a split sphere. Intersheet hydrogen-bonded linkages between donor and acceptor atoms are indicated by dotted blue lines (see text for discussion).

charge-balanced formula. Therefore, OH and/or H_2O groups must occur. We propose that the structure of cesbronite is an average structure that arises from the absence of correlation between sheets across a hydrogen-bonded interlayer. As we show below, it is possible to use bond-valence analysis to choose between the two ordering schemes and to identify the probable sites of protonation (OH groups) and arrive at a charge-balanced formula for cesbronite.

5.7. Oxygen atoms

In the following description we refer to the *M*—O1 bond as being 'long' compared with *M*—O2 and *M*—O3 bonds, which are shorter. However, we point out that when using the calculated position of a focus for the O1 atom displacement ellipsoid, the Te—O1 distance of 1.91 Å is actually around 0.04 Å shorter than the 'short' Te—O3 bonds (∼1.95 Å).

On average the O1 atom (found at apical corner sharing sites along the MO_6 chain) is bonded to $1Te_L + 2Cu_S + 1Cu_L$ and has a corresponding bond valence sum (BVS) of 1.743 v.u. (2.023 v.u. when calculated using the ellipsoid foci for Te_L and Cu_L). Thus, O1 is not protonated. We emphasise that there cannot be ordering involving quartets of $2Cu_S + 2Cu_L$, as this arrangement would require compensating $2Cu_S + 2Te_L$ quartets, which cannot occur due to the very high O1 BVS of 2.938 v.u. ($2 \times 0.449 + 2 \times 1.020$) that would arise. This condition holds true for both ordering schemes. Consequently, only the $1Te_L + 2Cu_S + 1Cu_L$ quartet can be bonded to O1.

The O2 atom (found at equatorial sites of the Cu1 atoms) forms two Cu_S—O bonds and has a BVS of 0.891 p.f.u. As such it is probably an OH group. This oxygen atom has a site multiplicity of 4, *i.e.* 2OH p.f.u. Thus, two more OH p.f.u. are still required for charge balance.

On average the O3 atom, found at equatorial *M* sites and apical Cu1 sites, is bonded to $1Te_S + 1Cu_S + 1Cu_L$ and has a corresponding BVS of 1.572 v.u. This bond triplet corresponds to ordering scheme (1) in which Te and Cu octahedra within a sheet (Fig. 6*a*). A BVS of 1.572 v.u. is far too high for the O3 bonded to this triplet to be an OH group.

For ordering scheme (2), in which Te and Cu of the mixed site occur as separate rows parallel to [100] of pure Te and pure Cu (Fig. 6*b*), there are two different local cation triplets bonded to O3: $2Cu_S + 1Cu_L$ and $2Te_S + 1Cu_L$. Their corresponding BVS values of O3 are 1.099 and 2.046 v.u., respec-

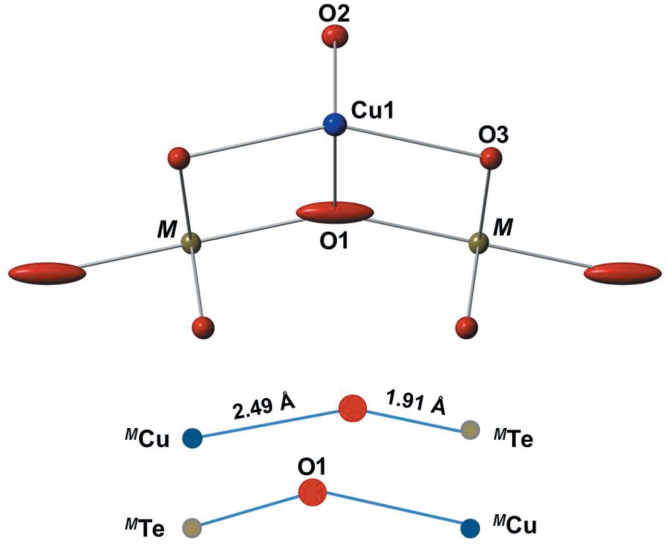

Figure 4
The environment of the O1 atom in cesbronite. All atoms shown with anisotropic displacement ellipsoids at the 68% level. The O1 ellipsoid is prolate with its long axis parallel to [001]. The lower two diagrams show the calculated Te—O1 and Cu—O1.

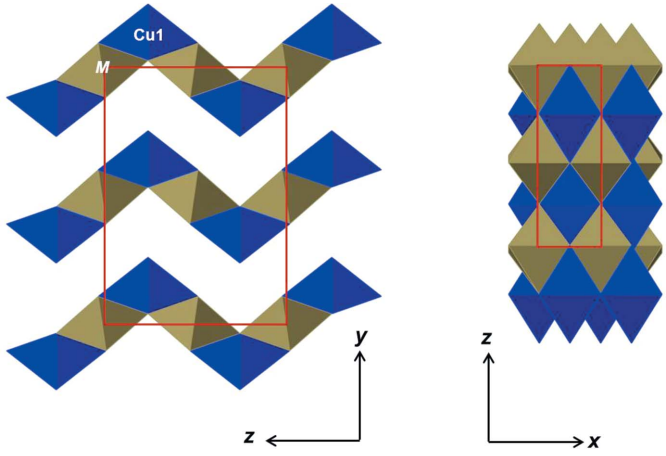

Figure 5
Polyhedral representations of the cesbronite average structure viewed down **x** and **y**, showing the corrugated layers formed by the octahedra and their superposition. The Cu1 octahedron is blue, and the *M* octahedron (50% Te and 50% Cu) is dark brown.

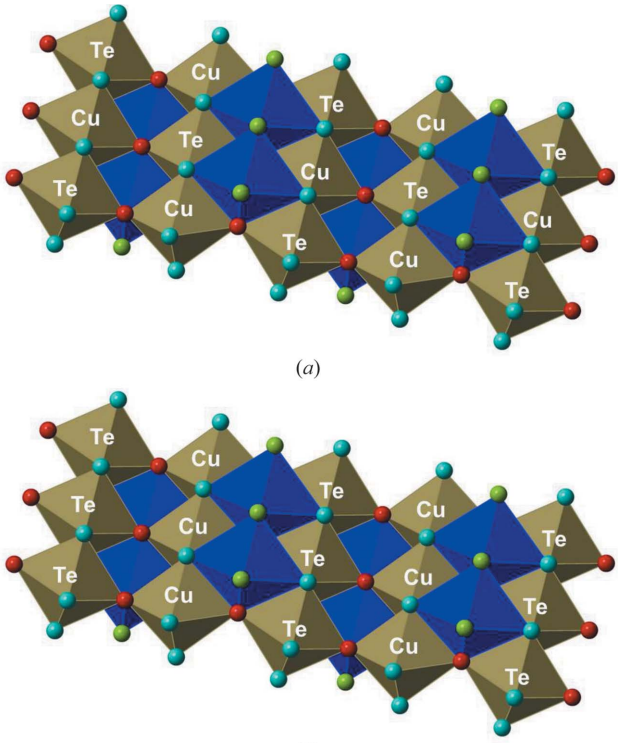

Figure 6
(*a*) Ordering scheme (1), looking down **a** with an angle of elevation of approximately 25°. Cu and Te alternate along a row parallel to [100]. (*b*) Ordering scheme (2), looking down **a** with an angle of elevation of approximately 25°. Cu and Te of the mixed site occur as separate, alternating Te and Cu [100] rows.

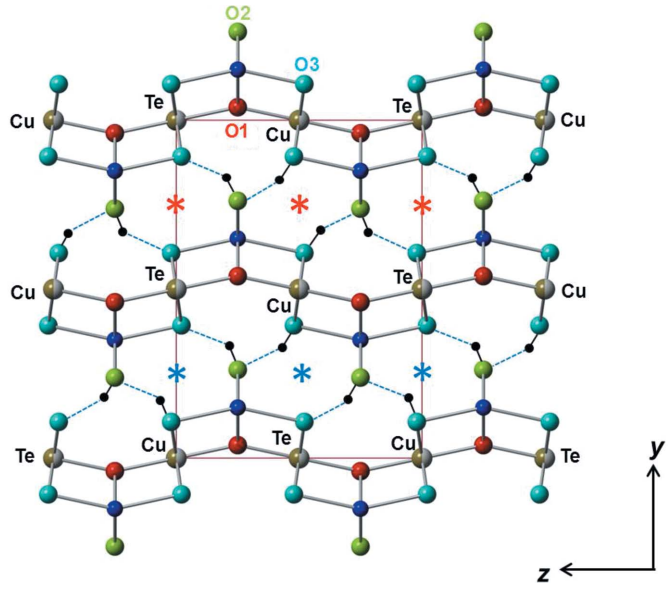

Figure 7
The local structure of cesbronite illustrating the two different interlayer hydrogen bonding configurations. Offsetting of polyhedral sheets involves *a*/2 translations. Red stars denote rings in which the two OH groups come from different polyhedral sheets that are not offset and lead to a *trans* arrangement and Cu—Cu and Te—Te cross-interlayer site superpositions. Blue stars denote rings in which the two OH groups come from the same polyhedral sheet and there is a *a*/2 offset that leads to a *cis* arrangement and Cu—Te cross-intersheet site superpositions. The structure is projected onto the **bc** plane and the unit cell of the average structure.

tively. Both values are plausible and the former value implies that O3 associated with Cu_3 triplets is OH, whereas the second triplet involves O, not OH. Thus, ordering scheme (2) is preferred. The site multiplicity of O3 is 8. However, only half of these sites are OH, *i.e.* those associated with the triplet Cu_3—OH. Consequently, O3 contributes four OH per unit cell and two OH p.f.u. Thus, O2 and O3 contribute a total of four OH to the cesbronite formula, leading to a charge-balanced formula $Cu_3TeO_4(OH)_4$.

Hence, bond valence analysis that takes into account preferred local cation configurations indicates clearly that there are two sites of protonation, O2 and O3, with the latter being 50% OH, 50% O in the average structure.

Fig. 7 shows schematically the two inter-sheet hydrogen-bonding configurations that, we propose, are sufficiently similar energetically so as to lead to lack of intersheet correlation parallel to [010] and complete stacking disorder of sheets in this direction. Note that OH groups are only associated with Cu atoms and the Te is bonded to O3 that is a hydrogen-bond acceptor when *M* = Te and donor (OH group) when *M* = Cu. One hydrogen-bonded interlayer consists of rings of *trans*-arranged OH groups (red stars in Fig. 7), whereas for the other interlayer has rings in which the pair of OH groups is *cis*-arranged (blue stars in Fig. 7). The *trans* configuration leads to the superposition of Cu—Cu and Te—Te atoms across the intersheet, whereas the *cis* configuration superimposes Cu and Te, across the intersheet, leading to the mixed site of the average structure. The $Cu_{0.5}Te_{0.5}$ composition of the mixed *M* site is consistent with a random stacking disorder of polyhedral sheets.

5.8. Relationship to other tellurium oxysalt structures

There is no exact analogue in the catalogue of 703 tellurium oxycompounds with crystal structures compiled by Christy, Mills & Kampf (2016) and Christy, Mills, Kampf *et al.* (2016). Cesbronite is closest in topology to the structures of $Ag_4[Cu(TeO_6)]$ (Klein *et al.*, 2007) and $Tl_4[Cu(TeO_6)]$ (Yeon *et al.*, 2012), numbers 507 and 508, respectively. These structures both have a chain framework, $[Cu(TeO_6)]^{4-}$, with a 1–2–1–2 arrangement of edge-linked CuO_6 octahedra, formed by TeO_6 octahedra edge-sharing with CuO_6 octahedra on alternating sides of the chain. Despite this apparent similarity, these chains form only a one-dimensional chain as opposed to an infinite sheet. None of the infinite layer structures of Christy, Mills & Kampf (2016) and Christy, Mills, Kampf *et al.* (2016) displays structural features remotely similar to cesbronite.

5.9. Relationship of cesbronite to xocomecatlite

The formula for cesbronite, $Cu^{II}{}_3Te^{VI}O_4(OH)_4$, is identical to that reported for xocomecatlite (Williams, 1975). We have recently determined that the unit cell of xocomecatlite from a crystal obtained from the cotype specimen BM 1976,404 is triclinic with cell parameters *a* = 7.33 (1), *b* = 13.04 (2), *c* =

14.17 (3) Å and $\alpha = 82.6$ (1), $\beta = 83.9$ (1) and $\gamma = 90.1$ (1)°, $V = 1335$ (4) Å^3, showing that it is a phase distinct from cesbronite (Missen, 2017). This unit cell fits perfectly the powder pattern given by Williams (1975), and is different from the 'possible' cell reported ($a = 12.140$, $b = 14.318$, $c = 11.662$ Å, $\alpha = 90$, $\beta = 90$, $\gamma = 90°$ and $V = 2027.1$ Å^3). Microprobe data for xocomecatlite show that its probable formula is $Cu_3TeO_6{\cdot}nH_2O$, $n \leq 1$ (Missen, 2017).

Acknowledgements

We thank Brendan Abrahams (University of Melbourne) for his insightful comments on the manuscript; Finlay Shanks (Monash University) for his assistance in acquiring the Raman data; Jens Najorka (Natural History Museum, London) for help in acquiring the powder pattern; Simon Hinkley (Museums Victoria, Australia) for taking the picture of the M53919 cesbronite specimen (Fig. 1) and Robert Housley (California Institute of Technology) for advice and comments on the Raman spectrum.

Funding information

This study has been partly funded by The Ian Potter Foundation grant 'Tracking tellurium' to SJM and a Museums Victoria 1854 Student Scholarship awarded to OPM, which we gratefully acknowledge. Microprobe work was funded through Natural Environment Research Council grant NE/M010848/1 'Tellurium and Selenium Cycling and Supply' to Chris J. Stanley (Natural History Museum, London), which we also gratefully acknowledge.

References

Christy, A. G., Mills, S. J. & Kampf, A. R. (2016). *Mineral. Mag.* **80**, 415–545.
Christy, A. G., Mills, S. J., Kampf, A. R., Housley, R. M., Thorne, B. & Marty, J. (2016). *Mineral. Mag.* **80**, 291–310.
Degen, T., Sadki, M., Bron, E., König, U. & Nénert, G. (2014). *J. Powder Diffr.* **29**, S13–S18.
Eby, R. K. & Hawthorne, F. C. (1993). *Acta Cryst.* B**49**, 28–56.
Frost, R. L. & Keeffe, E. C. (2009). *J. Raman Spectrosc.* **40**, 866–869.
Gagné, O. C. & Hawthorne, F. C. (2015). *Acta Cryst.* B**71**, 562–578.
Gaines, R. V. (1970). *Mineral. Rec.* **1**, 40–43.
Grundler, P. V., Brugger, J., Meisser, N., Ansermet, S., Borg, S., Etschmann, B., Testemale, D. & Bolin, T. (2008). *Am. Mineral.* **93**, 1911–1920.
Kampf, A. R., Cooper, M. A., Mills, S. J., Housley, R. M. & Rossman, G. R. (2016). *Mineral. Mag.* **80**, 1055–1065.
Kampf, A. R., Housley, R. M. & Marty, J. (2010). *Am. Mineral.* **95**, 1548–1553.
Kampf, A. R., Housley, R. M., Mills, S. J., Marty, J. & Thorne, B. (2010). *Am. Mineral.* **95**, 1329–1336.
Kampf, A. R., Mills, S. J., Housley, R. M., Rossman, G. R., Marty, J. & Thorne, B. (2013*a*). *Am. Mineral.* **98**, 1315–1321.
Kampf, A. R., Mills, S. J., Housley, R. M., Rossman, G. R., Marty, J. & Thorne, B. (2013*b*). *Am. Mineral.* **98**, 1617–1623.
Kampf, A. R., Mills, S. J. & Rumsey, M. S. (2017). *Mineral. Mag.* **81**, 1125–1128.
Kampf, A. R., Mills, S. J., Rumsey, M. S., Dini, M., Birch, W. D., Spratt, J., Pluth, J. J., Steele, I. M., Jenkins, R. A. & Pinch, W. W. (2012). *Mineral. Mag.* **76**, 1175–1207.
Klein, W., Curda, J. & Jansen, M. (2007). *Z. Anorg. Allg. Chem.* **633**, 231–234.
Kraus, W. & Nolze, G. (1996). *J. Appl. Cryst.* **29**, 301–303.
Laugier, J. & Bochu, B. (2004). *Chekcell*. http://www.CCP14.ac.uk/tutorial/lmgp/.
Mills, S. J. & Christy, A. G. (2013). *Acta Cryst.* B**69**, 145–149.
Mills, S. J., Kampf, A. R., Christy, A. G., Housley, R. M., Rossman, G. R., Reynolds, R. E. & Marty, J. (2014). *Mineral. Mag.* **78**, 1325–1340.
Missen, O. P. (2017). Masters Thesis, Department of Chemistry, University of Melbourne, Australia.
Pasero, M. (2017). The New IMA List of Minerals, http://nrmima.nrm.se/.
Rigaku Oxford Diffraction (2015). *CrysAlis PRO*. Rigaku Oxford Diffraction, Yarnton, England.
Roberts, A. C., Gault, R. A., Jensen, M. C., Criddle A. J. & Moffatt, E. A. (1997). *Mineral. Mag.* **61**, 139–144.
Sheldrick, G. M. (2008). *Acta Cryst.* A**64**, 112–122.